
**Liquid Crystals**
Publication details, including instructions for authors and subscription information:
http://www.informaworld.com/smpp/title~content=t713926090

# Anomalous relaxation of a twisted cell under an external magnetic field: The nearly homogeneous relaxation

Luca Carlotti[a]; Sandro Faetti[b]; Maurizio Nobili[a]
[a] Dipartimento di Fisica dell'Università di Pisa, Pisa, Italy [b] Istituto Nazionale di Fisica della Materia, Dipartimento de Fisica dell'Università di Pisa, Italy

**To cite this Article** Carlotti, Luca , Faetti, Sandro and Nobili, Maurizio(1996) 'Anomalous relaxation of a twisted cell under an external magnetic field: The nearly homogeneous relaxation', Liquid Crystals, 20: 6, 721 — 729
**To link to this Article: DOI:** 10.1080/02678299608033165
**URL:** http://dx.doi.org/10.1080/02678299608033165

LIQUID CRYSTALS, 1996, VOL. 20, NO. 6, 721–729

# Anomalous relaxation of a twisted cell under an external magnetic field: the nearly homogeneous relaxation

by LUCA CARLOTTI, SANDRO FAETTI*† and MAURIZIO NOBILI

Dipartimento di Fisica dell'Università di Pisa, Piazza Torricelli 2, 56126 Pisa, Italy
†Istituto Nazionale di Fisica della Materia, Dipartimento de Fisica dell'Università di Pisa, Piazza, Torricelli 2, 56126, Italy

(*Received 17 July 1995; in final form 4 December 1995; accepted 16 December 1995*)

We report experimental and theoretical investigations of the dynamic behaviour of a $\pi/2$ twisted NLC layer in a magnetic field. When a magnetic field $H$ is applied in the layer plane at a suitable angle $\beta$ with respect to the easy axis on the first surface, the relaxation towards the equilibrium texture occurs through a slow decay of unstable textures. Depending on the values of $H$ and $\beta$, the relaxation of the system can be nearly homogeneous or strongly inhomogeneous. In this paper we restrict our attention to the case where the relaxation occurs in a nearly homogeneous way. The theoretical relaxation time $\tau_W$ of the unstable textures is found to depend strongly on the angle $\beta$ and on the amplitude of the magnetic field. The experimental dependence of $\tau_W$ on $H$ and $\beta$ is found to be in good agreement with the theoretical predictions. The relaxation process is extremely sensitive to small dishomogeneities of the director easy alignment on the surfaces. From the measured relaxation we are able to estimate a spread of 0·3° on the surface easy axes at a planar anchored SiO surface.



## 1. Introduction

The dynamic behaviour of nematic liquid crystals (NLC) under the influence of magnetic or electric fields has been the object of intense interest in the literature (see, for instance, the recent books [1, 2] and references therein). The dynamic behaviour is strongly dependent on the initial alignment of the director $\mathbf{n}(\mathbf{r})$ in the NLC sample with respect to the applied external field. Most of the theoretical and experimental work has been concerned with NLC planar layers. Before switching on the external field, the configuration of the director field is due to the interactions of the NLC with the two planar plates that bound the NLC layer. Usually, the two plates are treated by physico-chemical methods in such a way as to induce a uniform director orientation along an axis in the $x$–$y$ film plane or along the normal $\mathbf{z}$ to the film plane. In some other cases, the initial director alignment is characterized by a uniform twist of the director along the $z$-axis orthogonal to the plates and an electric field $\mathbf{E}$ is applied along the orthogonal $z$-axis. This latter configuration has found important applications in the field of electro-optic devices [3–5].

In this paper we study another interesting configuration that gives rise to a very rich and unusual dynamic behaviour. The initial alignment in the NLC layer is a uniform $\pi/2$ twist along the $z$-axis orthogonal to the two parallel plates and an external magnetic field $H$ is applied in the $x$–$y$ film plane. In this special geometry, the quantitative and qualitative dynamic behaviour of the system is strongly dependent on the orientation of the magnetic field in the layer plane. The angle $\beta$ between the magnetic field $H$ and the easy axis on the first plane surface of the layer plays a very important role. For $-\pi/2 < \beta < 0$ (see figure 1), the relaxation of the initial configuration towards the equilibrium configuration is everywhere homogeneous and occurs within a characteristic time $\tau_R$ that is of the same order of magnitude as that which characterizes the Fréederickzs geometry far from the threshold. For $0 < \beta < \pi/2$, the dynamic behaviour of the system is much more complex.

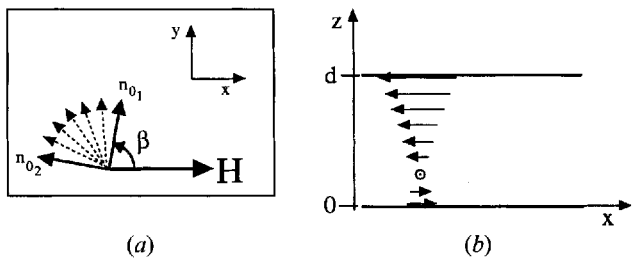


Figure 1. Director orientation in the pre-twisted NLC layer. $\mathbf{n}_{0_1}$ and $\mathbf{n}_{0_2}$ are the easy axes on the two plane surfaces. The magnetic field $H$ is applied parallel to the $x$-axis. $\mathbf{z}$ is the normal to the two plane surfaces positioned in $z = 0$ and $z = d$. (*a*) top view. (*b*) side view.

*Author for correspondence.

The relaxation towards the equilibrium is characterized by the occurrence of slow decay and unstable textures. Furthermore, in this latter case, in a given range of $\beta$ and $H$ values, the relaxation does not occur everywhere homogeneously, but some spatial textures are observed. We call this regime the *inhomogeneous relaxation.* For other values of $\beta$ and $H$, the relaxation of the system towards the equilibrium occurs in a nearly homogeneous way. We call this regime the *homogeneous relaxation.* Finally, the relaxation time $\tau_W$ is found to depend very strongly on the $\beta$-angle and to be much longer than $\tau_R$.

In this paper, we give a detailed theoretical and experimental analysis of the *homogeneous relaxation.* All the experimental observations are explained in terms of the well known Leslie–Ericksen hydrodynamic theory of NLCs. Finally, we show that the dynamic behaviour is extremely sensitive to the uniformity of the surface director alignment. The *inhomogeneous relaxation* will be the object of a forthcoming paper.

The plan of the paper is the following. In § 2 we introduce the dynamic equations; the numerical algorithm and the numerical solutions are given in § 2.1 and an approximate analytical expression of the relaxation time $\tau_W$ is given in § 2.2. In § 3 we illustrate the experiment; the experimental method and apparatus are shown in § 3.1 and the experimental results in § 3.2. Finally, in § 4 we draw the conclusions.



## 2. Dynamic equations of the director field

Let us consider a NLC cell with two plane parallel surfaces: surface 1 in $z = 0$ and surface 2 in $z = d$, where $\hat{\mathbf{z}}$ is the normal to the surfaces and $d$ is the cell thickness. $\phi$ is the angle between the director and an $\hat{\mathbf{x}}$-axis in a plane parallel to the surfaces. The easy directions $\mathbf{n}_{0_1}$ and $\mathbf{n}_{0_2}$ of the director on the two surfaces are in the plane of the surfaces and make angles $\beta$ and $\beta + \pi/2$ with respect to the $\hat{\mathbf{x}}$-axis, respectively, see figure 1 ($a$, $b$). The director goes from surface 1 with the surface angle $\phi_S = \beta$ to surface 2 with $\phi_S = \beta + \pi/2$ by making a twist distortion $\phi_0(z)$ given by:

$$\phi_0(z) = \beta + \frac{\pi}{2}\frac{z}{d}. \tag{1}$$

We are interested in the dynamic behaviour when a magnetic field $H$ parallel to the **x**-axis (see figure 1) is switched on at $t = 0$. The dynamical equation for the director is [1]:

$$\xi^2 \frac{\partial^2 \phi}{\partial z^2} - \frac{\sin(2\phi)}{2} = \tau_R \frac{\partial \phi}{\partial t}, \tag{2}$$

where we have introduced the magnetic coherence length $\xi$ given by:

$$\xi = \left(\frac{K_{22}}{\chi_\alpha}\right)^{1/2} \frac{1}{H}, \tag{3}$$

($K_{22}$ is the twist elastic constant and $\chi_\alpha$ is the diamagnetic anisotropy) and $\tau_R$ is a characteristic relaxation time which is given by:

$$\tau_R = \frac{\gamma_1}{\chi_\alpha H^2} = \frac{\gamma_1 \xi^2}{K_{22}}, \tag{4}$$

($\gamma_1$ is the bulk rotational viscosity coefficient). The initial and boundary conditions are given by:

$$\phi(z,0) = \beta + \frac{\pi}{2}\frac{z}{d}, \quad \phi(0,t) = \beta, \quad \phi(d,t) = \beta + \frac{\pi}{2}. \tag{5a,b,c}$$

In equations (5$b$) and (5$c$), we have assumed strong anchoring. In the bulk dynamical equation (2), we have omitted the backflow term, because its contribution is null in the twist geometry [6].

At the equilibrium, $\partial\phi/\partial t = 0$ and the equation (2) reduces to:

$$\xi^2 \frac{d^2\phi}{dz^2} - \frac{\sin(2\phi)}{2} = 0, \tag{6}$$

with the boundary conditions (5$b$) and (5$c$). Equation (6) can also be obtained by minimizing the total free energy per unit surface area given by:

$$f = \int_0^d F\,dz, \tag{7}$$

where $F$ is the free energy density:

$$F = \frac{K_{22}}{2}\left(\frac{d\phi}{dz}\right)^2 - \frac{\chi_\alpha}{2} H^2 \cos^2\phi. \tag{8}$$

In the following we consider the range of $\beta$-angles $\pi/4 < \beta < \pi/2$. In this range, the stationary texture, that we call 'texture (1)' is given by the expression:

$$\begin{cases} \dfrac{z}{\xi} = \displaystyle\int_\beta^\phi \frac{d\phi'}{[\frac{1}{2}(\cos 2\phi_{max} - \cos 2\phi')]^{1/2}} & \text{for } 0 \leqslant z \leqslant d_1, \\ \dfrac{z - d_1}{\xi} = -\displaystyle\int_{\phi_{max}}^\phi \frac{d\phi'}{[\frac{1}{2}(\cos 2\phi_{max} - \cos 2\phi')]^{1/2}} & \text{for } d_1 \leqslant z \leqslant d, \end{cases} \tag{9}$$

where $\phi_{max}$ is given by the integral:

$$\int_\beta^{\phi_{max}} \frac{d\phi'}{[\frac{1}{2}(\cos 2\phi_{max} - \cos 2\phi')]^{1/2}} - \int_{\phi_{max}}^{\beta + (\pi/2)} \frac{d\phi'}{[\frac{1}{2}(\cos 2\phi_{max} - \cos 2\phi')]^{1/2}} = \frac{d}{\xi}, \tag{10}$$

and $d_1$ is the $z$ coordinate, where $\phi(d_1)=\phi_{max}$. The equilibrium texture (I) is shown in figure 2. for $0<\beta<\pi/4$, the equilibrium texture is the symmetrical case of texture (I) with respect to the changes $\phi(z)\to\pi-\phi(z)$ and $z\to d-z$.

### 2.1. *Numerical solutions*

To find the numerical solution of equation (2) with the boundary conditions (5*a*), (5*b*) and (5*c*) we have used the PDECOL software package [7] in its double precision version. We have used the following values for the material parameters: $K_{22}=3{\cdot}27\times10^{-7}$ dyne [8], $\chi_a=1{\cdot}14\times10^{-7}$ [9], $\gamma_1=0{\cdot}72$ poise [10] that correspond to the nematic compound 4-pentyl-4′-cyanobiphenyl (5CB) at $T=25°C$.

In figure 3(*a–c*) is shown a 3D plot of the solution $\phi(z,t)$ versus $z$ and $t$ for $H=7{\cdot}7$ KG and $\beta=80°$. After $t=14\ \tau_R\approx1{\cdot}5$ s from the $H$ turn on, a $\pi$ twisted wall is formed in the bulk. The presence of a $\pi$-twisted wall can be explained in the following manner, if we call $z^*$ the point in the NLC layer where the director makes the angle $\phi(z^*)=\pi/2$ with the magnetic field. For $z<z^*$, $\phi(z)<\pi/2$ and the magnetic torque tends to orient the director parallel to $H$ ($\phi=0$). For $z>z^*$, $\phi(z)>\pi/2$ and the magnetic torque tends to orient the director antiparallel to $H$ ($\phi=\pi$). This means that the magnetic field generates a transient distortion having a $\pi$-wall close to position $z^*$. Details of the *appearance* of the $\pi$-wall are shown in figure 3(*b*). The $\pi$-wall texture remains nearly stationary for a very large time interval, then it rapidly relaxes after a time $\tau_W\approx600$ s towards the stable texture (I). Details of the time-interval when the $\pi$-wall disappears are shown in figure 3(*c*). To make clearer what 'very large' means, we must compare the relaxation time $\tau_W$ with the characteristic time $\tau_R$ defined in equation (4) which is $\tau_R=0{\cdot}1$ s for $H=7{\cdot}7$ KG. We should remark that by passing from the $\pi$-wall texture to the texture (I), the derivative $d\phi/dz$ at the surface $z=0$ changes its sign. Thus, the transition between the two textures can be controlled by measuring the sign of

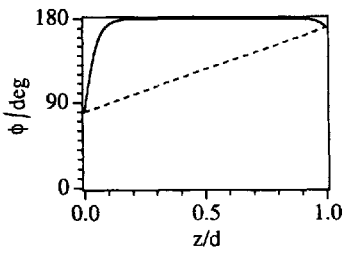


Figure 2. $\phi(z)$ versus $z/d$ for texture (I) and for $\beta=80°$ and $H=2{\cdot}5$ KG (i.e. $\xi/d=3{\cdot}47.10^{-2}$, solid line). The dashed line represents the initial distortion.

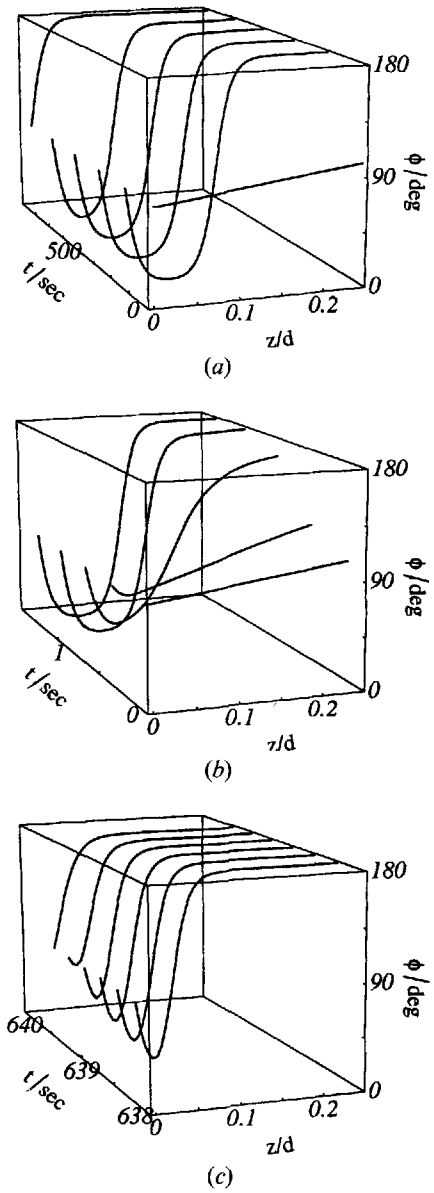


Figure 3. (*a*) $\phi(z,t)$ versus $z/d$ and $t$ for $H=7{\cdot}7$ KG and $\beta=80°$ when the magnetic field is switched on at $t=0$; (*b*) and (*c*) show details of (*a*) with the time scale expanded around $t=0$ and $t=640$ s, respectively. To obtain these numerical results we have used the material parameters: $K_{22}=3{\cdot}27.10^{-7}$ dyne [8], $\chi_a=1{\cdot}14.10^{-7}$ [9], $\gamma_1=0{\cdot}72$ poise [10].

$d\phi/dz$ in $z=0$ or the sign of the surface azimuthal torque $\Gamma_S=K_{22}(d\phi/dz)|_{z=0}$.

The $\pi$-wall appearance and its relaxation are two very different dynamic regimes. In figure 4(*a,b*) are shown the $\phi(z)$ profiles for $\beta=80°$, $H=7{\cdot}7$ KG and time intervals $t$ from field switching on in the ranges $0<t<14\tau_R$ and $14\tau_R<t<\tau_W$, respectively. For $0<t<14\tau_R$, in figure 4(*a*), the $\pi$-wall is formed at the initial position

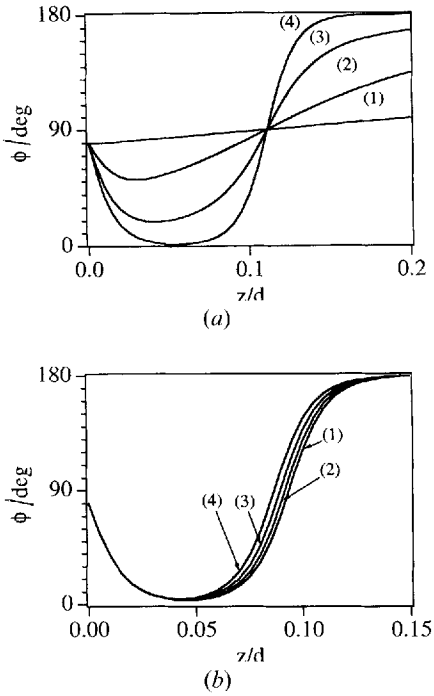


Figure 4. $\phi$ versus $z/d$ for $\beta = 80°$, $H = 7{\cdot}7$ KG and different time intervals $t$ from field switching on; (*a*) the curves shown correspond to (1) $t/\tau_R = 1$, (2) $t/\tau_R = 5$, (3) $t/\tau_R = 7$, (4) $t/\tau_R = 14$; (*b*) The curves shown correspond to (1) $t/\tau_W = 0{\cdot}81$, (2) $t/\tau_W = 0{\cdot}84$, (3) $t/\tau_W = 0{\cdot}875$, (4) $t/\tau_W = 0{\cdot}91$.

$z_i^*$ defined as $\phi_0(z_i^*) = \pi/2$, where $\phi_0$ is given by equation (1). The $\pi$-wall remains centred in $z_i^*$ during all its formation (i.e. $\phi(z_i^*)$ remains equal to $\pi/2$) while in all other points inside the cell, the director tends to orient parallel or antiparallel to the magnetic field. The director angle is an explicit function of time $t$: $\phi = \phi(z, t)$. For $14\tau_R < t < \tau_W$, in figure 4 (*b*), the $\pi$-wall shifts toward the surface $z = 0$. The temporal change of the $\phi(z)$ profile is due to the shift of the $\pi$-wall. In this regime, $\phi$ depends on time $t$ only through $z^*(t)$: $\phi = \phi(z, z^*(t))$.

Figure 5 shows a 3D plot of the disorienting azimuthal torque $\Gamma = K_{22}[(d\phi/dz)|_{z=0} - (\pi/2)(1/d)]$ at the surface $z = 0$ versus time $t$ and angle $\beta$ for $H = 1$ KG. We define $\tau_W$ as the time that is needed for $\Gamma$ to recover the initial value $\Gamma = 0$. Straight after switching on the field, for any value of $\beta$, $\Gamma$ goes toward negative values, i.e. the director field goes towards the texture with the $\pi$-wall. Then, after the relaxation time $\tau_W$, $\Gamma$ rapidly increases towards the positive values, reaching a stationary positive value that corresponds to texture (I). For $\beta \approx 90°$ the $\pi$-wall texture rapidly relaxes toward the stationary texture (I) and $\tau_W$ is very small. In the opposite case, for $\beta \approx 45°$, the $\pi$-wall texture remains stable for a long time before relaxing toward texture (I): $\tau_W$ is very large and it goes to infinity for $\beta = 45°$ (in the absence of thermal noise).

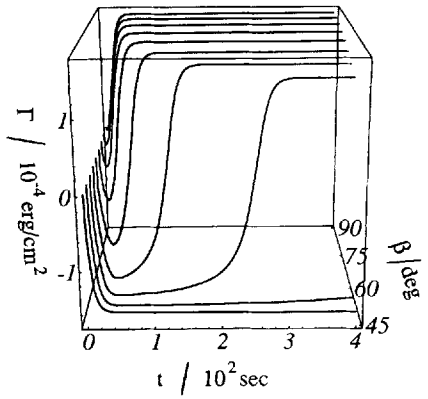


Figure 5. The disorienting azimuthal torque $\Gamma$ versus time $t$ and angle $\beta$ for $H = 1$ KG. The material parameters are the same as in figure 3.

It is important to remark here that numerical results in figure 5 relate to a somewhat small value of the magnetic field. For higher magnetic fields, the $\pi$-wall texture appears to be much more stable and the relaxation time can greatly increase. In particular, there is a large range of $\beta$ and $H$ values where the transient $\pi$-wall remains stable for a very large time. In this region of parameters $\beta$ and $H$ a simple approximated analytical expression of $\tau_W$ can be obtained. This analytical solution will be derived in the next sub-section and will be compared with the numerical results.

### 2.2. *Analytical determination of* $\tau_W$

For time intervals $\tau_R \ll t \ll \tau_W$ and in the range $3\xi < z^* < d - 3\xi$, the numerical solution of equation (2) can be accurately approximated by the analytical function:

$$\tan\frac{\phi}{2} = A\exp\left[-\frac{z}{\xi}\right] + \frac{1}{B\exp\left[\dfrac{(z^*-z)}{\xi}\right] + C\exp\left[-\dfrac{(d-z)}{\xi}\right]}, \tag{11}$$

where constants $A$, $B$ and $C$ are obtained by imposing the boundary conditions: $\phi(0) = \beta$, $\phi(z^*) = \pi/2$ and $\phi(d) = \beta + \pi/2$. We find for the three constants:

$$A \approx \tan\left[\frac{\beta}{2}\right] - \exp\left[-\frac{z^*}{\xi}\right], \tag{12a}$$

$$B \approx 1 + \tan\left[\frac{\beta}{2}\right]\exp\left[-\frac{z^*}{\xi}\right] - \cot\left[\frac{\beta}{2} + \frac{\pi}{4}\right]\exp\left[-\frac{d - z^*}{\xi}\right], \tag{12b}$$

$$C \approx \cot\left[\frac{\beta}{2}+\frac{\pi}{4}\right]-\exp\left[-\frac{d-z^*}{\xi}\right]. \qquad (12c)$$

To obtain the constant values in equations (12*a*), (12*b*) and (12*c*) we have disregarded terms of higher order in $\exp[-z^*/\xi]$ and $\exp[-(d-z^*)/\xi]$. Figure 6 shows the numerical solution (points) and the approximated function (solid line) for $H = 7{\cdot}7$ KG, $\beta = 80°$ (i.e. $z^*/\xi = 7{\cdot}2$ and $d/\xi = 88{\cdot}6$) and $t/\tau_W = 0{\cdot}15$. One can see that the approximate solution (11) reproduces the numerical profile very well. In particular, we can verify that the discrepancy between the numerical and the analytical solutions is everywhere smaller than $\exp[-(2z^*)/\xi] \approx 6.10^{-7}$. By injecting the analytical solution (11) in the free energy density per unit surface area $f$ equation (7), after some tedious calculation we obtain the generalized force $F_W = -(\partial f)/(\partial z^*)$ on the $\pi$-wall given by:

$$F_W \approx -\frac{8K_{22}}{\xi^2}\left(\tan\left[\frac{\beta}{2}\right]\exp\left[-\frac{z^*}{\xi}\right] - \tan\left[\frac{\pi}{4}-\frac{\beta}{2}\right]\exp\left[-\frac{d-z^*}{\xi}\right]\right). \qquad (13)$$

In (13) we have disregarded terms of order higher than $\exp[-(z^*/\xi)]$ and $\exp[-(d-z^*)/\xi]$. The initial position of the $\pi$-wall $z_i^*$ and the surface angle $\beta$ are linked by the equation:

$$z_i^* = \left(1-\frac{2\beta}{\pi}\right)d. \qquad (14)$$

If $\beta = \pi/4$ we have $z_i^* = (d/2)$ from (14) and $F_W = 0$ from (13). The force on the $\pi$-wall is zero at the switching on of the magnetic field and it remains zero always. Indeed, in this case, the relaxation time $\tau_W$ goes to infinity if one does not account for the thermal noise. Moreover if $\beta > \pi/4$, we have from (14) $z_i^* < (d/2)$ and the first term in (13) is larger than the second one ($\exp[-z^*/\xi] > \exp[-(d-z^*)/\xi]$); thus $F_W < 0$ and the $\pi$-wall is pushed towards the first surface ($z = 0$). Exactly the opposite happens for $\beta < \pi/4$: the force on the $\pi$-wall is positive and the wall relaxes toward the second surface in $z = d$. For $\pi/4 < \beta < \pi/2$ and $z^* < d/2 - 3\xi$, the second term in (13) is negligible with respect to the first and $F_W$ can be approximated by:

$$F_W \approx -\frac{8K_{22}}{\xi^2}\tan\left[\frac{\beta}{2}\right]\exp\left[-\frac{z^*}{\xi}\right]. \qquad (15)$$

To calculate the relaxation time of the $\pi$-wall, we make the hypothesis that the wall velocity $v_W(z^*) = dz^*/dt$ is proportional to the force on the wall [11]:

$$F_W(z^*) = \gamma_W v_V(z^*), \qquad (16)$$

where $\gamma_W$ is a friction coefficient per unit surface area of the $\pi$-wall. The $\gamma_W$ coefficient can be evaluated in the following manner. The wall movement with speed $v_W$ entails a local director rotation with angular speed $\partial\phi/\partial t$. By assuming that the wall shift does not excite the fluid flux, the director rotation is accompanied by an entropy production per unit surface area $\sigma$ given by [12]:

$$\sigma = \gamma_1 \int_0^d \left(\frac{\partial\phi}{\partial t}\right)^2 dz. \qquad (17)$$

By comparing $\sigma$ (17) to the total rate of energy dissipation $F_W v_W = \gamma_W v_W^2$ [13], we obtain for $\gamma_W$ the following expression:

$$\gamma_W = \frac{\gamma_1}{v_W^2}\int_0^d \left(\frac{\partial\phi}{\partial t}\right)^2 dz. \qquad (18)$$

From figure 4(*b*) we see that, for $t \gg \tau_R$, when the $\pi$-wall is already formed, the time dependence of $\phi$ is entirely due to the $\pi$-wall movement, i.e. we have $\phi(z,t) = \phi(z, z^*(t))$. In this regime the $\phi$ time derivative is given by: $(\partial\phi)/(\partial t) = (\partial\phi)/(\partial z^*)v_W$ and the $\gamma_W$ expression (18) writes:

$$\gamma_W = \gamma_1 \int_0^d \left(\frac{\partial\phi}{\partial z^*}\right)^2 dz. \qquad (19)$$

By substituting the approximate expression (11) for $\phi(z)$ in (19) and by neglecting contributions of the order of $\exp[-z^*/d]$, we obtain the simple relationship:

$$\gamma_W \approx \frac{2\gamma_1}{\xi}. \qquad (20)$$

This result is also expected from a dimensional analysis. In fact $\gamma_W$ has the dimension of $\gamma_1$ divided by a length and the only characteristic length of the wall is its thickness $\xi$.

The relaxation time $\tau_W$ is obtained from the integral:

$$\tau_W = \int_0^{\tau_W} dt \approx \int_0^{z_i^*} \frac{dz^*}{|v_W(z^*)|}. \qquad (21)$$

From equations (15), (16), (20) and (21) we obtain for

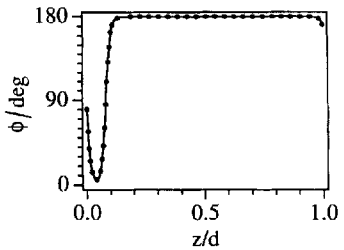


Figure 6. $\phi(z)$ versus $z/d$ for $H = 7{\cdot}7$ KG, $\beta = 80°$ and $t/\tau_W = 0{\cdot}15$. The points represent the numerical results; the solid line shows the approximate analytical profile equation (11).

$\tau_W$:

$$\tau_W \approx \frac{\xi^2 \gamma_1}{4K_{22}\tan\left[\frac{\beta}{2}\right]}\left(\exp\left[\frac{z_i^*}{\xi}\right]-1\right). \qquad (22)$$

By using equation (14) for $z_i^*$, we obtain:

$$\tau_W \approx \frac{\xi^2 \gamma_1}{4K_{22}\tan\left[\frac{\beta}{2}\right]}\exp\left[\left(1-\frac{2\beta}{\pi}\right)\frac{d}{\xi}\right]. \qquad (23)$$

$\tau_W$ depends nearly exponentially on the surface angle $\beta$, with an exponential characteristic coefficient given by $-(2d)/(\pi\xi)$, i.e. linear in the magnetic field amplitude.

In figure 7 is reported $\tau_W$ versus the angle $\beta$ in a semi-logarithmic scale. The points represent the $\tau_W$ values obtained by the numerical integration of equations (2), (5 *a*), (5 *b*) and (5 *c*) for two $H$ values; the straight lines represent the theoretical expression (23). The analytical expression reproduces very well the numerical results in the limit of the surface angles far from $\pi/2$ ($z_i^* \gg 0$).

It can be interesting to compare the $\pi$-wall relaxation time $\tau_W$ in (23) with the typical relaxation time $\tau_R$ of the director in a magnetic field (4). By substituting $\tau_R$ (4) in (23), we find:

$$\tau_W \approx \frac{\tau_R}{4\tan\left[\frac{\beta}{2}\right]}\exp\left[\left(1-\frac{2\beta}{\pi}\right)\frac{d}{\xi}\right]. \qquad (24)$$

Due to the presence of the exponential factor, $\tau_W$ can become many orders of magnitude higher than $\tau_R$. This means that the $\pi$-wall texture behaves as an almost stationary configuration for the director field. This is clearly visible in figure 7 where characteristic times of $10^3$ s are reached by the system, whilst $\tau_R = 0{\cdot}93$ s at $H = 2{\cdot}6$ KG. This strong dependence of the relaxation time $\tau_W$ on angle $\beta$ is somewhat similar to the dynamical behaviour of a system close to a second order transition

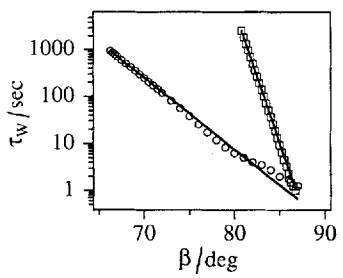


Figure 7. Semi-logarithmic plot of the $\pi$-wall relaxation time $\tau_W$ versus angle $\beta$ for $H = 10$ KG (i.e. $\xi/d = 8{\cdot}68.10^{-3}$, upper curve) and $H = 2{\cdot}6$ KG (i.e. $\xi/d = 3{\cdot}34.10^{-2}$, lower curve). The points represent the numerical results; the solid lines represent the predictions of the expression (23).

with the difference that, in this latter case, the slowing down is characterized by a critical exponent.

We conclude our theoretical analysis by remarking that our theoretical results have been obtained by assuming a perfect uniform orientation of the director on the two interfaces and the absence of thermal noise. With these assumptions, the director-field is a function of $z$ only and does not depend on the position in the layer plane. Therefore, in this case, the relaxation towards the equilibrium state can occur in a homogeneous way. The presence of some small surface dishomogeneities of the local easy axes can have very important consequences on the macroscopic behaviour of the system. Indeed, according to equation (24) and to figure 7, the relaxation time $\tau_W$ strongly depends on the $\beta$ angle. This means that, if $\beta$ is not exactly the same in any point of the NLC interfaces, $\tau_W$ becomes a function of the $x$–$y$ coordinates that can exhibit strong variations from point to point. In this case the director-field is expected to be a function of $x$, $y$ and $z$ (inhomogeneous behaviour). This inhomogeneous behaviour will be discussed in a forthcoming paper.

## 3. Experimental

### 3.1. *Experimental method and apparatus*

To compare the theoretical results with experiment, we have made a cell consisting of two glass plates filled with the NLC 5CB. The two glass plates are treated by SiO evaporation. The SiO thickness $s_{SiO}$ and the SiO evaporation angle $\alpha_{SiO}$ are: $s_{SiO} = 450$ Å and $\alpha_{SiO} = 60°$, well inside the planar anchoring region of the $\alpha_{SiO} - s_{SiO}$ phase diagram [14]. In this way, the nematic easy axis is in the plane of the surface and perpendicular to the evaporation plane. The two glass plates are mounted with the easy axes perpendicular to each other, so that a uniform twist distortion of the total angle about 90° is present in the cell. The sign of the twist is not important for the phenomena described above. If the twist angle is $-90°$ in place of the $+90°$ twist angle considered in the theoretical analysis, all theoretical results can be still obtained by changing $\beta \to -\beta$. In the following, we will consider a NLC cell with a $+90°$ twist angle, but similar results have also been obtained for a $-90°$ twist angle.

To characterize the NLC patterns, we use a reflectometric method [15]. A 5 mW He–Ne laser beam is polarized by a polarizer which makes an angle $\alpha_P$ with the magnetic field and impinges at almost normal incidence on the NLC layer (see figure 8). To separate the laser beams reflected from the various interfaces, we make the cell with two glass plates sandwiched at the ends by two mylar spacers having different thickness (130 μm and 260 μm) in such a way as to make a wedge. The glass plates too are wedge shaped, with a wedge

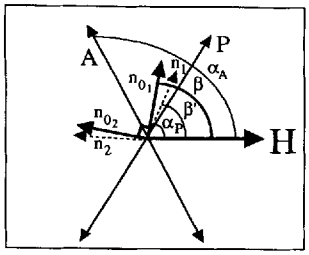


Figure 8. Top view of the cell with polarizer orientations. Polarizer P and analyzer A make the angles $\alpha_P$ and $\alpha_A$ with respect to the magnetic field $H$, respectively. The solid vectors $\mathbf{n}_{0_1}$ and $\mathbf{n}_{0_2}$ represent the easy directions at the first and the second interface, respectively. $\beta$ is the angle between $\mathbf{n}_{0_1}$ and $H$. The dashed vectors $\mathbf{n}_1$ and $\mathbf{n}_2$ represent the surface directors in the first transient regime after the switching on of $H$. $\beta'$ is the angle between $\mathbf{n}_1$ and $H$.

angle 0·4°. Under these conditions the laser beams reflected from the first SiO–NLC interface can be easily separated from the other reflected beams. The NLC is kept at the temperature $T = 25°C$ and lies between the two polar expansions of a Brucker electromagnet giving a magnetic field up to 7·7 KG. The temperature is stabilized within $\pm 0{\cdot}01°C$. The laser beam reflected from the first SiO–NLC interface passes through an analyser which makes an angle $\alpha_A$ with the magnetic field given by $\alpha_A = \alpha_P + \pi/2$ (crossed polarizer and analyser) and is collected by a photodetector. The reflected light intensity $I(t)$ after the analyser is:

$$I(t) = I_0 \sin^2[2(\phi_S(t) - \alpha_P)], \tag{25}$$

where $\phi_S$ is the director angle at surface $z = 0$ with respect to the magnetic field direction, and $I_0$ is the maximum of the reflected light intensity measured between crossed polarizers [15]. When the magnetic field is switched on, the director at the surface rotates by an angle $\Delta\phi_S(t)$ towards the magnetic field. In the hypothesis of small surface rotations, $\Delta\phi_S(t) = \phi_S(t) - \beta \ll \beta$, the difference $\Delta I(t) = I(t) - I_0$ in the reflected light intensity before and after switching on the magnetic field writes as:

$$\Delta I(t) \approx 2I_0 \sin[4(\beta - \alpha_P)]\Delta\phi_S(t). \tag{26}$$

By keeping $\alpha_P = \beta - \pi/8$, we find for $\Delta\phi_S(t)$ the expression:

$$\Delta\phi_S(t) \approx \frac{\Delta I(t)}{2I_0}. \tag{27}$$

The measured angle variations $\Delta\phi_S$ at the maximum value of the magnetic field and at the temperature $T = 25°C$ are $\Delta\phi_S \approx 0{\cdot}6°$. This surface rotation is very small and, so, the theoretical results obtained with the assumption of strong anchoring satisfactorily describe our experimental conditions. In a time interval of about $\tau_R$ ($\tau_R \ll \tau_W$) after switching on the magnetic field, the surface torque reorients the surface director by an angle $\Delta\phi_S(H) < 0$. Therefore, the surface angle $\beta'$ (see figure 8) during the relaxation of the $\pi$-wall is given by:

$$\beta' = \beta + \Delta\phi_S(H). \tag{28}$$

Then, to compare the experimental results with the theoretical predictions, $\beta$ must be substituted with $\beta'$ in equations (23) and (24). The experimental error on the $\Delta\phi_S$ measurement is about 0·1°. The angle $\Delta\phi_S(t)$ is related to the first derivative of $\phi(z)$ at the nematic–SiO interface ($z = 0$) by the boundary equation [16]:

$$\Gamma_S = K_{22}\left.\frac{d\phi}{dz}\right|_{z=0} = \frac{\partial W(\phi_S)}{\partial\phi_S} \approx W_a\Delta\phi_S(t), \tag{29}$$

where $W(\phi_S)$ is the azimuthal anchoring energy and $W_a$ is the azimuthal anchoring coefficient [16]. By measuring $\Delta I(t)$, we can calculate $\Delta\phi_S(t)$ from (27) and, finally, with (29) the surface azimuthal torque $\Gamma_S$. In this way we are able to distinguish texture (I) which gives a positive $\Gamma_S$ from the $\pi$-wall texture which gives a negative $\Gamma_S$. Moreover, we can follow quantitatively the surface dynamics of the $\pi$-wall relaxation toward the stationary texture (I). In the theoretical analysis in §2, we considered a planar NLC cell, while in the experiment we used a wedge cell. The wedge geometry is needed to use the very sensitive reflectometric method. However, we have also made experiments with planar cells by using a less sensitive transmission technique. The response of these two kinds of cell to the magnetic field is the same. This means that the experimental behaviour is not appreciably affected by the wedge of the cell.

### 3.2. *Experimental results*

Figure 9 shows a 3D plot of the disorienting torque $\Gamma(t)$ versus $t$ and $\beta'$ for $H = 7{\cdot}7$ KG. $\Gamma(t)$ is obtained from the variation $\Delta I(t)$ of the reflected light intensity between crossed polarizers via eqations (27) and (29).

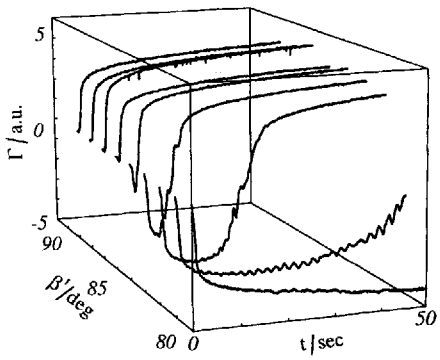


Figure 9. $\Gamma$ versus $t$ and $\beta'$ for $H = 7{\cdot}7$ KG.

$\beta'$ is given by the measured $\beta$ and $\Delta\phi_S$ via (28); $t = 0$ corresponds to the time of switching on the magnetic field. One can see that, for $\beta' \approx 90°$, $\Gamma(t)$ becomes rapidly greater than zero and the stationary texture (I) is formed almost instantaneously; however, for $\beta'$ far from 90°, the $\pi$-wall relaxation time $\tau_W$ becomes much longer. This behaviour is in agreement with the numerical results reported in figure 5.

To compare quantitatively the experimental results to the theoretical predictions, in figure 10 is reported the semi-logarithmic plot of $\tau_W$ versus $\beta'$ for $H$ values which go from $H = 0{\cdot}96$ KG to $H = 7{\cdot}7$ KG. We must remember that $\tau_W$ denotes the time that is needed for the disorienting torque $\Gamma(t)$ in figure 9 to recover the initial value $\Gamma(0) = 0$. The points are the experimental data; the solid lines represent the natural logarithm of $\tau_W$ (23) for the given magnetic field amplitudes.

By going more deeply into the comparison between the experimental measurements and the theoretical predictions, in figure 11 is reported $\Gamma(t)$ versus time $t$ for $H = 7{\cdot}7$ KG and $\beta' = 83{\cdot}5°$. The solid line represents the

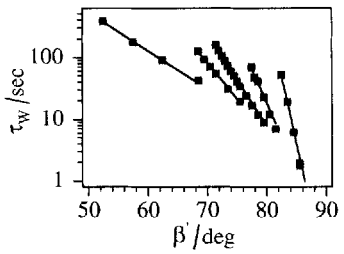


Figure 10. Semi-logarithmic plot of $\tau_W$ versus $\beta'$. The points represent the experimental measurements. The solid lines represent the predictions of the expression (23) when the material parameters are those in figure 3. The five curves correspond to five different magnetic field amplitudes, in particular from left to the right: $H = 0{\cdot}95$ KG, $H = 1{\cdot}95$ KG, $H = 2{\cdot}6$ KG, $H = 3{\cdot}9$ KG, $H = 7{\cdot}7$ KG. The temperature is $T = 25°$C.

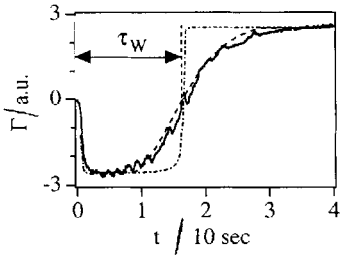


Figure 11. $\Gamma$ versus $t$ for $H = 7{\cdot}7$ KG and $\beta' = 83{\cdot}5°$. The solid line represents the experimental measurements. The dot-dashed line represents the theoretical curve obtained by integrating equation (2). The dashed line represents the theoretical curve obtained by supposing that the surface is made up from different portions having slightly different orientations of the easy axis distributed over a gaussian curve of average $\beta' = 83{\cdot}5°$ and width $\Delta\beta' = 0{\cdot}3°$.

experimental points, the dot-dashed line represents the numerical curve obtained by integrating the equation (2) with $\beta' = 83{\cdot}5°$. We see clearly that, although the theory gives the correct value of the characteristic time $\tau_W$, the experimental time dependence of $\Gamma(t)$ is very different from the theoretical. This discrepancy can be explained by accounting for the very great dependence of the relaxation time $\tau_W$ on the $\beta'$-angle. This strong dependence makes the relaxation very sensitive to small dishomogeneities of $\beta$, i.e. of the easy axis of the director, and of $\Delta\phi_S$, i.e. of the anchoring energy of the surface. To explain the experimental results shown in figure 11, we assume that the director orientation at the surface of the NLC and the anchoring strength are not everywhere the same, but some spread of easy directions and anchoring strengths exists. Therefore the measured relaxation is the superposition of the different relaxations at different points of the NLC layer. This assumption is also confirmed by a direct analysis of the NLC layer with a polarizing microscope using transmitted light. Figure 12($a$, $b$) shows the NLC layer before and after switching on the magnetic field. In figure 12($b$) we see clearly spatial regions of different contrast. This observation is clear evidence for the fact that relaxation towards the equilibrium state does not occur homogeneously.

To obtain a theoretical expression for the relaxation of this system, we have supposed that the illuminated area ($\approx 1$ mm$^2$) of the NLC layer is made up of 101 small domains having different values of $\beta'$ distributed according to a gaussian distribution with width $\Delta\beta'$. Then, the total response of this system is obtained as the superposition of the dynamical behaviour of each surface domain. The dashed line in figure 11 represents the numerical curve obtained from the integral:

$$\begin{cases} \Gamma(t) = \displaystyle\int_{\bar\beta' - 0{\cdot}5°}^{\bar\beta' + 0{\cdot}5°} G(\beta')\Gamma(\beta', t)\,\mathrm{d}\beta' \\ G(\beta') = \dfrac{1}{(2\pi)^{1/2}\Delta\beta'} \exp\left[ -\dfrac{1}{2}\left(\dfrac{\beta' - \bar\beta'}{\Delta\beta'}\right)^2 \right], \end{cases} \tag{30}$$

where $\bar\beta' = 83{\cdot}5°$, and $\Gamma(\beta', t)$ is the theoretical response of a single domain oriented at the angle $\beta'$. From the best fit of the experimental curve we find an angular spread on $\beta'$: $\Delta\beta' = 0{\cdot}3°$. Thus, by looking at the form of the surface dynamical signal we are able to estimate the amplitude of the surface static noise on the easy axis directions and on the anchoring strengths.

## 4. Conclusion

In this paper we report experimental and theoretical investigations of the dynamic behaviour of a twisted NLC layer in a magnetic field parallel to the layer plane.

(*a*)

(*b*)

Figure 12. Image of the NLC layer between parallel polarizers observed using the polarizing microscope. The polarization of the incident beam is at the angle $\alpha_P = 75°$ with the easy axis on the first interface of the NLC layer. (*a*) and (*b*) show the NLC layer before and after switching on the magnetic field, respectively.

Due to the presence of an initial $\pi/2$ uniform twist of the director field, the approach of the system to the equilibrium is somewhat complex and slow decay, transitory textures are observed.

The static and dynamic behaviour is found to depend greatly on the angle $\beta$ between the magnetic field and the easy direction in the layer plane of the first interface. If $-\pi/2 < \beta < 0$, the relaxation toward the equilibrium occurs in a time $\tau_R$ of the same order of magnitude as that which characterizes the Fréedericksz geometry far from the threshold. In the opposite case of $0 < \beta < \pi/2$, the relaxation of the system is characterized by the occurrence of nearly stable textures. Now, the relaxation time $\tau_W$ depends very strongly on the angle $\beta$ and it can become much larger than $\tau_R$. For somewhat high values of the magnetic field amplitude, $\tau_W$ can change by some orders of magnitude if $\beta$ changes by a few degrees. This special feature makes the dynamic response extremely sensitive to the uniformity of the surface alignment. In this paper we have restricted our analysis to those regions in the $\beta - H$ space where the spatial inhomogeneities do not strongly affect the qualitative dynamical behaviour of the system. From the measured relaxation, we have estimated a spread $\Delta\beta \approx 0{\cdot}3°$ on the surface easy axis at a planar anchored SiO surface.

The experimental results are obtained using an optical reflectometric method. All the experimental results are explained quantitatively by the Leslie–Ericksen hydrodynamic theory of NLCs. The dependence of the relaxation time $\tau_W$ on the magnetic field $H$ and on the angle $\beta$ is in a good agreement with the theoretical predictions.

For certain values of parameters $\beta$ and $H$, the dynamical behaviour of the system becomes much more complex and is characterized by a strongly inhomogeneous behaviour with the occurrence of spatial domains separated by walls or disclination lines. The theoretical and experimental investigations of this behaviour will be given in a forthcoming paper.

## References


[1] DE GENNES, P. G., and PROST, J., 1993, *The Physics of Liquid Crystals*, 2nd Edn. (Oxford: Clarendon Press).

[2] CHANDRASEKHAR, S., 1992, *Liquid Crystals*, 2nd Edn. (Cambridge: Cambridge University Press), p. 88.

[3] SCHADT, M., and HELFRICH, W., 1971, *Appl. Phys. Lett.*, **18**, 127.

[4] SCHEFFER, T. J., and NEHRING, J., 1984, *Appl. Phys. Lett.*, **45**, 1021.

[5] WATERS, C. M., BRIMMEL, V., and RAYNES, E. P., 1983, in Proceedings of the 3rd International Display Research Conference, Kobe, Japan, p. 396.

[6] BROCHARD, F., PIERANSKI, P., and GUYON, E., 1973, *J. Phys. (Paris)*, **34**, 35.

[7] MADSEN, N. K., and SINCOVEC, R. F., 1979, *ACM Trans. Math. Software*, **5**, 326.

[8] GATTI, M., FAETTI, S., and PALLESCHI, V., 1985, *J. Phys. (France) Lett.*, **46**, 881.

[9] SCHERREL, P. L., and CRELLIN, D. A., 1979, *J. Phys. Colloq.*, **40**, C3-213.

[10] COLES, H. J., and SEFTON, M. S., 1976, *Mol. Cryst. liq. Cryst. Lett.*, **36**, 51.

[11] CLADIS, P. E., VAN SAARLOOS, W., FINN, P. L., and KORTAN, A. R., 1987, *Phys. Rev. Lett.*, **58**, 222.

[12] IMURA, H., and OKANO, K., 1973, *Phys. Lett.*, **42A**, 403.

[13] RYSKIN, G., and KREMENETSKY, M., 1991, *Phys. Rev. Lett.*, **67**, 1574.

[14] BOIX, M., MONKADE, M., and DURAND, G., 1988, *Europhys. Lett.*, **5**, 697.

[15] PALLESCHI, V., FAETTI, S., and SCHIRONE, A., 1988, *Il Nuovo Cimento*, **10**, 1313.

[16] NOBILI, M., FAETTI, S., and SCHIRONE, A., 1991, *Liq. Cryst.*, **10**, 95.